Joint Centre for Mesoscale Meteorology, Reading, UK

Correction for Attenuation of Radar Reflectivity using Polarisation Data

T. J. Smyth
A. J. Illingworth

Internal Report No. 89

June 1998

Met Office Joint Centre for Mesoscale Meteorology Department of Meteorology
University of Reading PO Box 243 Reading RG6 6BB United Kingdom
Tel: +44 (0)118 931 8425 Fax: +44 (0)118 931 8791
www.metoffice.com

Designed and produced by the Met Office © Crown copyright 2001 01/0240 The Met Office logo is a registered trademark.

Correction for Attenuation of Radar Reflectivity using Polarisation Data.

T. J. Smyth*and A. J. Illingworth

JCMM, Department of Meteorology, University of Reading, UK

April 29, 1998

* Current affiliation: Tim Smyth, Plymouth Marine Laboratory, Prospect Place, Plymouth PL1 3DH. email: T.J.Smyth@pml.ac.uk

Abstract

Attenuation by heavy rain is a major operational problem in radar estimation of rainfall rates which is increasingly severe at wavelengths shorter than 10cm. Gate-by-gate correction algorithms, including those using both reflectivity (Z_H) and differential reflectivity (Z_{DR}), are inherently unstable. In addition values of Z_H and Z_{DR} are affected by hail, which causes little attenuation. Methods dependent upon differential phase shift (K_{DP}) do not give unique solutions but depend upon rain drop size distributions. A new technique which uses both K_{DP} and differential attenuation between the horizontally and vertically polarised radiation (A_{H-V}) is proposed. The total A_{H-V} is measured from the negative Z_{DR} in light precipitation behind the attenuating region. Theory and observation show that corrections based on the K_{DP} -A_{H-V} scheme should be unaffected by hail, stable and accurate. A simpler algorithm may be feasible at C-band in which the total attenuation is derived from the observed total differential attenuation. It appears that the most severe case of attenuation result from heavy rain consisting of large oblate raindrops. Accordingly, the attenuation would be appreciably reduced if operational radars used vertical polarisation rather than the commonly employed horizontal polarisation.

1 Introduction

If reliable rainfall rates for regions of intense precipitation are to be calculated using radar, then correction for attenuation is necessary. Attenuation becomes increasingly more serious as the wavelength is reduced. At S-band ($\lambda = 10$cm) the effect has previously been considered to be negligible (Hitschfeld and Bordan, 1954) , whereas at C-band ($\lambda = 5$cm; the wavelength of many operational radars in Europe) attenuation due to precipitation is well known to disrupt rainfall rate estimation. The gate-by-gate attenuation correction scheme of Hitschfeld and Bordan (1954) which relies on a relationship between attenuation, A, and reflectivity, Z, is known to be very unstable and, as shown by Hildebrand (1978), extremely sensitive to calibration errors. Delrieu *et al.* (1991) have computed relationships between A and Z for different wavelengths, temperatures and drop size distributions assuming the raindrops to be spherical. They show that at C-band the attenuation at 20°C is typically about 75% of the value at 0°C , and, for example, that for a 100mmhr^{-1} rainfall rate and 0°C they predict that different drop size distributions can give one way attenuations ranging from 0.43 to 0.67dBkm^{-1} . For airborne radar the "stereoradar" technique (Kabeche and Testud, 1995) relies on observing precipitation cells from two angles. A very simple version of this technique could be used when two neighbouring radars in a network provide overlapping coverage; it is most unlikely that the paths from both radars will suffer attenuation so only the unaffected beam is used. However, for most operational networks such overlapping regions are not widespread. Recently, Delrieu *et al.* (1997) reported a ground-based version of the "surface reference technique" developed for spaceborne radars. This method, using an X-band radar in mountainous terrain, relies on measuring the reflectivity of a well defined distant clutter target when there is attenuation to estimate the path integrated attenuation, and then using this as a constraint for the gate-by-gate retrieval. Such a technique may be appropriate at X-band where attenuation is so very severe, but the accuracy is limited for example by the day to day variation of about 3dB in the apparent reflectivity of the clutter target in dry weather.

This paper presents observations made of a severe convective event on the 7 June 1996, which caused severe differential attenuation (A_{H-V}) between the horizontally and vertically polarised copolar returns of up to 5dB, by the S-band Chilbolton multiparameter radar in Southern England. Rapid response raingauges, situated 500m below the precipitation region causing the radar attenuation, measured values in excess

of 250mmhr^{-1} . A numerically stable algorithm to correct for reflectivities measured with horizontal and vertical polarisations is proposed which relies on both A_{H-V} and differential phase shift (ϕ_{DP}).

2 Definition of Radar Parameters.

Differential reflectivity is defined as (Seliga and Bringi, 1976) :

$$Z_{DR} = 10log_{10}\frac{Z_H}{Z_V} \qquad (dB) \tag{1}$$

where Z_H and Z_V are the backscattered reflectivity in the horizontal and vertical polarisations respectively. Z_{DR} is a measure of the reflectivity weighted oblateness (Jameson, 1983) . Raindrops are oblate to a degree which increases with size, and fall with their minor axis oriented vertically. Rain can therefore be described as an anisotropic medium. High positive values of Z_{DR} are associated with large oblate raindrops.

The one way absolute attenuation, using the formulation of Oguchi (1973), is defined as,

$$A_H = 8.686 \times 10^3 \lambda \int Im\left[S_{fH}(D_e)\right] N(D_e) dD_e \qquad (dBkm^{-1}) \tag{2}$$

where $Im(S_{fH}(D_e))$ (in m) is the imaginary component of the forward scatter amplitude in the horizontal polarisation. When dual polarisation radar illuminates a region filled with oblate spheroids oriented with their minor axes vertical, such as in rain, the horizontal polarisation will become attenuated to a greater extent than the vertical. This is known as differential attenuation, A_{H-V} , and is defined as,

$$A_{H-V} = 8.686 \times 10^3 \lambda \int Im\left[S_{fH}(D_e) - S_{fV}(D_e)\right] N(D_e) dD_e \qquad (dBkm^{-1}) \tag{3}$$

A factor of two is required in 2 and 3 to account for two way attenuation. A_{H-V} can be deduced by the magnitude of negative Z_{DR} in light precipitation behind an attenuating region. In these regions Z_{DR} should be close to zero as the raindrops will be approximately spherical. For example, if Z_{DR} is -2dB in light rain then the total path integrated A_{H-V} along the ray is 2dB.

The differential phase shift, ϕ_{DP} , is the difference in phase between the copolar radar returns measured with vertical and horizontal polarisation ($\phi_V - \phi_H$). ϕ_{DP} is made up of three contributions; propagation (K_{DP}), differential phase shift on backscat-

ter (δ) and a hardware offset (ϕ_o).

$$\phi_{DP}(r) = 2\int_0^r K_{DP}(r)dr + \delta(r) + \phi_o \qquad (°), \tag{4}$$

where r is the range. K_{DP} is the propagation component of ϕ_{DP} as a function of range, and is defined as:

$$K_{DP} = 2 \times \frac{180 \times 10^3 \lambda}{\pi} \int Re\left[S_{fH}(D_e) - S_{fV}(D_e)\right] N(D_e) dD_e \qquad (° \text{ km}^{-1}) \tag{5}$$

where S_{fH} and S_{fV} are the forward scattering amplitudes (in m) for horizontally and vertically polarised waves, the factor of two is for two-way propagational differential phase shift and the factor of 10^3 is a conversion from ° m^{-1} to ° km^{-1} . As the incident wave propagates through a region of rain the horizontally polarised wave lags progressively behind the vertical one, because raindrops display a high degree of anisotropy. This causes a positive differential phase shift. In rain the value of K_{DP} is approximately proportional to the rain-rate, R. A relationship of the form

$$K_{DP} = 0.03R^{1.15} \qquad (° \text{ km}^{-1}) \tag{6}$$

at S-band has been proposed by Sachidananda and Zrnić (1986). At S-band, the differential phase shift on the backscatter component of ϕ_{DP} , δ , is usually considered to be very small as it only occurs in the Mie regime, that is for raindrops of size 7mm and rather larger for dry hailstones, and is only measurable if the hydrometeors have a preferred orientation (McCormick *et al.*, 1979) , but not if randomly oriented. It is important to note that δ , being a backscatter effect, is a transitory change in ϕ_{DP} superposed on the general propagation effect, and can introduce ambiguity in the interpretation of the signal. The observed δ for a distribution of scatterers in the pulse volume can be calculated using the cross correlation coefficient ρ_{HV},

$$\rho_{HV} = \frac{\int S_{bH}(D_e) S^*_{bV}(D_e) N(D_e) dD_e}{\left[\int |S_{bH}|^2 N(D_e) dD_e\right]^{1/2} \left[\int |S_{bV}|^2 N(D_e) dD_e\right]^{1/2}} \tag{7}$$

$$\rho_{HV} = |\rho_{HV}| \, exp(j\delta) \tag{8}$$

where $S_{bH,V}$ is the backscatter in the horizontal/vertical and the units of δ are in radians.

3 Attenuation Correction Algorithms.

a) Single parameter

Several attenuation correction algorithms have been derived and implemented on both actual and simulated data. The simplest algorithms involve the use of reflectivity (Z) only data (see e.g., Hitschfeld and Bordan (1954) and Hildebrand (1978)), are generally gate-by-gate iterative schemes and prove to be highly numerically unstable. The UK Met. Office (UKMO) attenuation correction scheme is a cumulative gate-by-gate algorithm of the form

$$A = 0.0044R^{1.17} \qquad (\mathrm{dBkm}^{-1}) \tag{9}$$

for the two way attenuation (Collier, 1990) based on the work of Gunn and East (1954). This procedure is prone to instability and so the predicted correction is capped and the maximum correction factor allowed is a doubling of the rainfall; this will be used operationally for all UK radars from 1998 and is similar to that in use in Sweden and Spain (A. Smith, UKMO, *pers comm*). A great deal of the instability in single parameter schemes is caused by initial radar calibration (Hitschfeld and Bordan, 1954) . Z only schemes are also unable to distinguish between rain and hail (because $Z \propto D^6$, where D is the particle diameter, and contains no information about the composition of the precipitation volume) which could lead to spurious amounts of correction via the conversion to rain rate.

b) Dual parameter

Aydin *et al.* (1989) formulated a theoretical correction algorithm for use at C-band using a combination of Z_H and Z_{DR} . From the premise that R estimates are improved by using the Z_H and Z_{DR} pair, it is a natural progression to the assumption that the introduction of Z_{DR} should improve estimates of attenuation. Using drop size distributions (DSDs) obtained by distrometer measurements they modelled backscattering and extinction cross sections to obtain the radar parameters of Z_H , Z_{DR} , and calculate A_H and A_{H-V} . They derived empirical relationships between A_H or A_V and the Z_H , Z_{DR} pair using a least squares polynomial fit. A gate-by-gate scheme was employed to produce a first order correction and an iteration process invoked at the nth gate which was repeated until the absolute difference between two consecutive approximations of Z_H and Z_{DR} at that gate were less than 0.1 and 0.05dB respectively. They found however that those conditions were satisfied within one iteration. To test for noise and biases they simulated radar data and found that any bias in Z_H deteriorated that procedure because the errors add cumulatively. Scarchilli *et al.* (1993) used a similar scheme but they parametrised A_H and A_{H-V} in terms of Z_H and Z_{DR} .

Tan (1995) describes a scheme which does not rely upon a gate-by-gate iterative technique and is therefore highly numerically stable. Instead a compensation method is used which uses relationships between A_H , A_V and the Z_H , Z_{DR} pair. This is illustrated in figure 1 and relies on the negative slope of the A_H /Z_H against Z_{DR} curve. The effect of attenuation will be to reduce the observed value of both Z_H and Z_{DR} . If the attenuated value of Z_{DR} is used rather than the true value of Z_{DR} , then the negative value of the slope in figure 1 means that the computed value of A_H /Z_H is larger than it should be. However, if when evaluating A_H /Z_H we use the observed attenuated value of Z_H , then the resultant predicted value of A_H will be close to the true one. The errors of using the attenuated values of both Z_H and Z_{DR} thus tends to cancel out and the calculated value of A_H is closer to the true one than if Z_H alone had been used.

The technique then is to use the uncorrected values of Z_H and Z_{DR} and to predict a value of A_H at each gate. This value of A_H is then used at each gate to correct Z_H on a gate-by-gate basis. When Z_{DR} becomes very small the scheme is difficult to implement because of the increasingly steep slope of the curve in figure 1. If the attenuation is so large that Z_{DR} becomes negative then an alternative approach is needed. Tan (1995) suggests using a relationship between A_H and A_{H-V} ,

$$A_{H-V} = A_H - A_V \qquad (dBkm^{-1}) \tag{10}$$

$$A_H \simeq 2.95 \times A_{H-V} + 0.084 \qquad (dBkm^{-1}) \tag{11}$$

this relationship being empirical and unique to C-band. An iterative step is invoked if any negative values of Z_{DR} remain.

The fundamental difficulty with all Z_H -Z_{DR} schemes is the assumption that only rain is present. When hail occurs, then Z_H increases and Z_{DR} falls and such schemes will erroneously infer exceptionally heavy rain consisting of small drops with consequently spurious high levels of attenuation.

c) Differential phase scheme

ϕ_{DP} is ideally suited for use in an attenuation correction algorithm because it has similar features to A_H and A_{H-V} . Both are forward scatter effects; the real part of the forward scatter amplitudes is proportional to K_{DP} whereas the imaginary part is proportional to attenuation. ϕ_{DP} itself is not affected by attenuation as it measures the difference in phase, and also it is relatively unaffected by hail. An additional factor is that raindrops become more oblate with increasing size implying that K_{DP} increases

with increased specific differential attenuation which implies that there is some form of relationship between the two parameters.

The use of ϕ_{DP} to correct for attenuation was first suggested by Bringi *et al.* (1990) and their calculations have been re-worked in section 5. They suggested the use of linear relationships between K_{DP} and both A_H and A_{H-V} . As will be shown in section 5 the use of a single linear relationship is equivalent to assuming a constant value of D_0 but allowing N_0 to vary in the standard exponential raindrop size distribution e.g.,

$$N_0(D) = N_0 exp(\frac{-3.67 \times D}{D_0}) \qquad m^3 mm^{-1} \tag{12}$$

where D_0 is the equivolumetric diameter which divides the volume of the spectra into two equal halves, and N_0 is the intercept of the curve on the N_0 axis. In their simulations Bringi *et al.* (1990) did not allow D_0 to rise above 2.5mm, a very low value for heavy precipitation.

4 Observations

In this paper we propose a method of correcting for attenuation which involves ***both*** differential phase shift and the accumulated differential attenuation (i.e., negative Z_{DR} on the far side of the storm). An example is shown in figure 2 where the differential attenuation and differential phase shift are clearly visible behind shafts of heavy rain. The "stripes" of negative Z_{DR} and phase shift emanate from a region behind an intense rainfall shaft (where Z_{DR} is $>$ 4dB) in a manner analogous to a shadow, pointing to the region where attenuation is occurring. Two regions of A_{H-V} are apparent from figure 2 along radials of 270° and 240° . Also shown in figure 2 are the positions of two rapid response drop counting gauges (g5 and g7) which provided 30 second resolved rain rate estimates.

Ryzhkov and Zrnić (1994) draw attention to the existence of differential attenuation accompanying large values of differential phase shift. Although the ray profile they show is very noisy with 50° noise on ϕ_{DP} and 1dB on Z_{DR} , they present a statistical analysis suggesting the amount of A_{H-V} for a given ϕ_{DP} is about twice as much as predicted by Bringi *et al.* (1990).

5 Scattering Calculations

a) Hail

The scattering coefficients for hailstones of various structural compositions, i.e., dry, spongy (30% water-ice mixture), covered with a layer of water, were extracted using the T-matrix Waterman (1965) code and the effect of shape and alignment investigated. The dielectric constants for water and ice were those calculated by Ray (1972) and Liebe *et al.* (1989). Dry hail (hail above the melting layer) was modelled using the dielectric constant of dry ice (3.15 + 0.0004i; at 0°C and λ=9.75cm). In all cases there is no air contained in the mixture. Spongy hail contains water within a frozen ice lattice and can be considered to be a homogeneous mixture of the two; the dielectric constant can be extracted using the Bruggemann rule (O'Brien and Geodecke, 1988) . Wet hail was modelled using both the dielectric constant of water (79.082 + 25.351i; at 0°C and λ=9.75cm) and using two-layer calculations which essentially considered a central ice core embedded within a water shell, 0.01cm thick (Atlas *et al.*, 1960) .

The concentration of the hailstones was modelled using the exponential DSD empirically derived by Cheng and English (1983);

$$N(D_e) = 115\gamma^{3.63} e^{-\gamma D_e} \qquad (m^{-3}mm^{-1}) \tag{13}$$

where D_e is in mm. Using the hail data, Cheng and English found that γ did not fall outside the range of 0.1 - 2.0mm^{-1}.

Figure 3 shows a comparison between the amounts of A_H resulting from spherical hailstones, and Marshall-Palmer (MP) (N_0 = 8000 m^{3}mm^{-1} in 12) rainfall. The hail data points in figure 3 refer to the different physical compositions. Within each physical category γ in 13 is varied between 0.1 - 2.0mm^{-1}. These calculations which are displayed in figure 3 suggest that at S-band most attenuation is produced when Z_H >60dBZ and that the hail contributes very little to the attenuation because it is present in such low concentrations. Because of these low concentrations, the K_{DP} of hail is much less than that of rain even if it is wet, aligned and oblate.

b) Rain.

To model the effect of rain, a normalised gamma DSD (14) was used (Blackman, 1996) in preference to the gamma DSD and its associated relationships proposed by Ulbrich (1983).

$$N(D_e)dD_e = \frac{N_0}{|\mu|!}(\Gamma D_e)^{\mu} e^{-\Gamma D_e} dD_e \qquad (m^{-3}) \tag{14}$$

$$\Gamma = \frac{(3.67+\mu)}{D_0} \qquad (mm^{-1}) \tag{15}$$

where D_0 (mm) is the median diameter of the DSD, N_0 the concentration of the drops ($m^{-3}mm^{-1}$) and D_e their equivolumetric diameter; μ describing the form of the distribution. Studies using radar have found μ to vary between 0 and 5 (Wilson *et al.* (1997)), and 2 and 4 (Illingworth and Caylor (1989)). A distrometer study by Goddard and Cherry (1984) showed μ to be closer to 5. In this paper, to obtain the variability found in naturally occurring rain, we vary μ between 0 and 5 in the normalised gamma DSD of 14. The shapes of Beard and Chuang (1987) were used in preference to those of Green (1975) and Pruppacher and Pitter (1971); Caylor (1989) found that Beard and Chuang shapes gave the best approximation in naturally occurring rain to what was observed by the Chilbolton radar.

Figures 4 and 5 are a re-working of Bringi *et al.* (1990) calculations of the relationships between A_H and A_{H-V} against K_{DP} for various raindrop size spectra. Bringi *et al.* considered that a D_0 of 2.5mm was the maximum likely to occur. A D_0 of 2.5mm is equivalent to a Z_{DR} of 3dB, yet values of Z_{DR} up to 6dB are observed in rain, so in figures 4 and 5 we have extended values of D_0 up to 7mm and truncated the spectrum at 10mm. (The curves plotted are for pure exponentials with μ=0.) Whereas Bringi *et al.* found a single relationship linking K_{DP} to the two attenuation coefficients, the inclusion of larger mean drop sizes leads to a family of curves predicting higher attenuation for a given K_{DP} .

K_{DP} , A_H and A_{H-V} are all proportional to N_0 (2, 3 and 5), so in figures 4 and 5 lines of constant D_0 are straight lines through the origin with N_0 varying along the straight line. The proposed single linear relationship of Bringi *et al.* between K_{DP} and both A_H and A_{H-V} , is then equivalent to assuming that in attenuating rainfall D_0 is constant and equal to 2.5dB, and Z_{DR} (when corrected for attenuation) is constant in the rain at 3dB.

Also shown in figures 4 and 5 are the lines of constant N_0. Showing, for example, that the D_0=7mm initially intercepts the N_0=8$m^{-3}mm^{-1}$ and then, when K_{DP} =18° km^{-1} , N_0=80$m^{-3}mm^{-1}$. The graph for N_0=8$m^{-3}mm^{-1}$ corresponds to a low concentration of increasingly large raindrops and the line is terminated when the value of D_0 is so big that the rainfall rate be comes unrealistically large. Because the spectra are truncated at 10mm these high D_0 spectra are effectively almost monodispersed containing only very large raindrops. It needs to be noted that the relationships shown in figure 4 and

5 are sensitive to changes in μ. However, for the purposes of attenuation correction outlined in section 6 these effects are small.

The only difference between the calculations of K_{DP} and A_H for a given N_0, D_0 and μ, ignoring the constant terms, is that K_{DP} is proportional to the real part of the forward scatter amplitude whereas A_H is proportional to the imaginary part. Therefore any differences between the two parameters should become apparent when the scattering coefficients are studied closely. Figure 6 provides an explanation of the behaviour shown in figure 4. Once the raindrop size is larger than 3mm the real part of the forward scatter amplitude increases less rapidly than the imaginary part. This means that there is more attenuation for a given phase shift for the larger drops, confirming the trend in figures 4 and 5. In physical terms, figure 4 suggests that the greatest amount of attenuation is caused by a small number of large drops being present within the radar volume. The implication follows that there are not simple linear relationships between attenuation and K_{DP} . Any method purporting to correct for total attenuation must have information on both the N_0 and D_0 of the rainfall spectrum causing the attenuation.

Attenuation is strongly dependent upon temperature (Jameson, 1992) , this is because the attenuation rate is controlled by molecular absorption and scatter out of the beam. Molecular absorption (the imaginary component) is enhanced at lower temperatures plus the fact that molecular absorption is dominant at the frequencies of 3 and 5GHz over almost all raindrop sizes. This is shown in figure 7. At 20°C the value of $Im(S_{fH})$ is 40% less than when the temperature is 0°C over a large range of the raindrop sizes. This implies that when using model results to correct for attenuation great care must be taken in selecting a representative temperature for the raindrops.

6 Correction Scheme

The attenuation correction algorithm proposed in this paper which uses the two propagation observables, K_{DP} and the total amount of A_{H-V} , is outlined in figure 8. The total amount of A_{H-V} is estimated from the negative Z_{DR} beyond the intense precipitation and is partitioned amongst the gates where K_{DP} >1° km^{-1} with a weighting proportional to the magnitude of K_{DP} . Values of N_0 and D_0 are derived from A_{H-V} and K_{DP} (as in figure 5) at each gate and A_H is computed at that gate. The corrected values of Z_H and Z_{DR} are then found from A_H and A_{H-V} at each gate. The highest

values of attenuation occur in the regions of low N_0 and high D_0 and are only slightly affected by changes in the assumed value of μ.

The values of N_0 and D_0 are uniquely defined in K_{DP} /A_{H-V} space, if the value of μ in the DSD is predetermined, and the value of A_H can be computed at each gate. There are small errors in estimating A_H in this manner because the lines of constant N_0 and D_0 are almost parallel in K_{DP} /A_{H-V} space, as shown in figure 5, for $D_0 < 7$mm. This means that for a fixed value of A_{H-V} and allowing K_{DP} to vary (to simulate random errors in the measurement of ϕ_{DP}), changes in D_0 are compensated for by changes in N_0. Table 1 highlights this point for a fixed A_{H-V} of 0.25dBkm^{-1} . For example, if the value of K_{DP} is 15$\pm$2° km^{-1} (realistic measurement error), then the associated value of A_H for a fixed A_{H-V} =0.25dBkm^{-1} is 0.37$\pm$0.04dBkm^{-1} . In other words a 14% error in the measurement of K_{DP} will lead to a 11% error in the estimated value of A_H . If the total attenuation suffered by the beam is of the order of 5dB, to have corrected Z_H to within 0.5dB is more than satisfactory as it corresponds to an accuracy of derived rainfall rate of better than 10%.

Once the individual gate's value of A_H and A_{H-V} are known, the corrected values of Z_H and Z_{DR} can be extracted by cumulatively summing the attenuation parameters. This scheme is not numerically unstable as any error at a particular gate does not contribute to successive gates, unlike iterative gate-by-gate methods. The scheme is also physically based; the measured parameters being used to compute components of the DSD, rather than relying upon a mathematical compensation effect as in the scheme of Tan (1995); also it is insensitive to hail which should not contribute to A_{H-V} or K_{DP} . However within the scheme there are flaws. For one particular attenuation event A_{H-V} is divided between the gates depending upon the K_{DP} weighting thus the attenuation corrected points are constrained upon a line of constant D_0, the coincidental values of N_0 being allowed to vary. This is easier to envisage with the aid of figure 5. D_0 is in effect defined over the whole precipitation core responsible for the attenuation rather than allowing for any gate-to-gate variation which is possible within heavy storms over short spatial scales.

Comparing tables 1 and 2 shows that the scheme is insensitive to μ variation for the purposes of calculating A_H from the K_{DP} , A_{H-V} pair. There appears to be a compensation effect between D_0 and N_0 with the result that there is only a 2.5% difference between the A_H calculated using μ=0 and that using μ=2. A fixed value of

μ can therefore be used within the scheme.

Figure 9 shows that most of the data points lie along the line of N_0=800$m^{-3}mm^{-1}$ with a D_0 of between 2.5 and 5mm. The maximum value of D_0 used in the calculations of Bringi *et al.* was 2.5mm. These results show that larger values of D_0 need to be considered and that the drop size spectrum should include raindrops of diameters up to 8 or 10mm. There is a considerable departure from the $A_H = 0.016K_{DP}$ line in figure 9 which suggests that a different linear relationship exists for each value of D_0; this is consistent with the theoretical scattering calculations presented in figures 4 and 5. In short the precise composition of the DSD has a large bearing upon the relationship between K_{DP} and the attenuation parameters, especially when it comprises of a low number concentration of large drops, and this is the advantage of implementing the attenuation algorithm detailed above. The scheme essentially defines a N_0, D_0 pair for a fixed value of μ in K_{DP} /A_{H-V} (A_H) space and therefore is an improvement upon simply relating K_{DP} to the attenuation parameters with no knowledge of the DSD. We have assumed that at S-band δ is negligible. In operational terms the scheme assigns a value of D_0 to an entire rain shaft, thus fixing a linear relationship between K_{DP} and A_{H-V} which is unique to that particular core. The value of N_0 is not constrained and is allowed gate-to-gate variability through the rain shaft.

The values of total differential phase shift, ϕ_{DP} , at S-band when there is attenuation occurring are quite large. Goddard *et al.* (1994) propose a method of self-calibration of Z_H to within 0.5dB using the consistency of Z_H , Z_{DR} and K_{DP} in rain. This method, has been used to calibrate Z_H for the data in this study. It relies on the fact that K_{DP} /Z_H as a function of Z_{DR} is virtually independent of μ in the DSD. The technique involves adjusting the Z_H calibration until the ϕ_{DP} calculated from the measured Z_H and Z_{DR} agrees with that observed. Provided the ϕ_{DP} used for calibration is limited to 30° , attenuation of Z_H and Z_{DR} is negligible and the method is reliable.

7 Results and Validation

Figure 10 shows the fields of Z_H and Z_{DR} along the azimuth containing gauge 7 (see figure 2), which is situated at a range of 32.2km. The measured Z_{DR} shows negative values at the back of the storm of -1.5dB, implying that the total amount of A_{H-V} through the storm is 1.5dB. The total amount of A_H is impossible to ascertain by simple inspection, it can only be obtained by calculation. The attenuation is occurring

over three major precipitation cores centred at 25, 50 and 65km from Chilbolton, with the greatest amount ~1dB occurring at the closest precipitation shaft where the temperature is about 20°C (the temperature in figures 4 and 5). The correction to Z_{DR} has, by definition, removed the negative values in the region of light precipitation (the negative values of Z_{DR} between the radar and 20km are caused by ground clutter). It is the corrected Z_H , Z_{DR} pair values at each gate which are important for rainfall rate estimation. Only if both components are accurately corrected for will the rainfall rate estimate be meaningful; this can be tested for using *in situ* raingauges and statistical methods.

a) Raingauge

Over a single ray validation using a raingauge can be beneficial, although raingauge radar comparisons are fraught with difficulties such as point representivity, beam overshoot and precipitation wind drift. The correction algorithm can also only be truly validated if the raingauge is situated in a region affected by attenuation and if the gauge has a rapid time response as attenuation events are transitory. Gauge 7 was positioned in such a place at 1936UTC; gauge 5 was between the radar and gauge 7 in the region causing the attenuation. Figure 11 shows the rainfall rate trace of gauges 5 and 7. Gauge 5 was recording 267mmhr^{-1} at the time of the coincidental PPI scan; this was very close to the radar estimated R (assuming that hail was not present in the precipitation volume), using both Z_H (=58dBZ) and Z_{DR} (=2.6dB) (DSD spectrum truncated at 10mm), of 268mmhr^{-1} , although it must be emphasised that at such high reflectivities the estimation of R is very dependent upon the value of μ used within the DSD. There is evidence from the radar scan that hail is present in the immediate vicinity of gauge 5, resulting in spurious R estimations using Z_H and Z_{DR} . Regions of hail tend to give the radar signature of high Z_H and low values of Z_{DR} (Aydin *et al.*, 1986) , if the hail is tumbling i.e., appears to be anisotropic to the polarisation radar. If the radar signature is interpreted as being due to rain in these high Z_H low Z_{DR} regions the rain DSD equivalent is a high number concentration of small raindrops. As rainfall rate (R) is a volumetric effect then the result is a seeming large value of R.

Using the uncorrected values of Z_H and Z_{DR} over the position of gauge 7 gives an estimated rainfall rate of 10mmhr^{-1} (using μ=0), whereas the corrected value of R is 3.0mmhr^{-1} . There is a seeming paradox here in that the estimated rainfall rate has been reduced by correcting for attenuation. The reason for this is that the value of Z_{DR}

has been increased which effectively reduces the number of small raindrops within the volume. This effect would not have occurred if R had been estimated using Z_H alone; the corrected and uncorrected values would have been 7.5mmhr^{-1} and 4.7mmhr^{-1} respectively. The corrected value of R (3.0mmhr^{-1}) is within 10% of the gauge 7 recorded rainfall rate of 3.3mmhr^{-1} . On these results the attenuation correction algorithm appears to be effective.

b) Statistical

Using gauges to validate for attenuation correction schemes has a limited scope, especially where rain gauges are sparsely distributed. A better means of validation would be to check for internal "self consistency" within the scan. That is to compare regions affected by attenuation and those that are not in terms of Z_H and Z_{DR} . The scatterplots in figure 12 show remarkable detail as to the efficacy of the attenuation algorithm. The feature to note is the "bulge" of negative Z_{DR} in b) which indicates the need for attenuation correction. This is most pronounced between 10 and 25dBZ and for the correction algorithm to be judged successful these negative values must not only be removed, but they must be adequately redistributed such that the corresponding values of Z_H are reasonable. An attenuated azimuth is defined as a ray which contains negative Z_{DR} (outside of the clutter region), and it includes the unattenuated portions of the ray between the radar and the attenuating core. Qualitatively comparing a) and c), the background (that is azimuths unaffected by attenuation) and corrected azimuths respectively, shows the scheme to successfully correct for attenuation. The majority of the negative Z_{DR} has been removed, all that remains is due to clutter similar to the pattern in a). An interesting feature to note in b) and c) is the pairs of high Z_H (>55dBZ) and low Z_{DR} (<2dB), possibly being caused by hail. However it is only upon inspection of the scatterplot polynomials in d) that the scheme can truly be shown to correct to a high degree of accuracy, in the cases examined, for both Z_H and Z_{DR} ; this being the vital factor for rainfall rate estimation. The corrected polynomial results in a curve similar in shape and form to the background fit. The coefficients of the second order polynomial fits provide a more quantitative comparison between the separate data sets, shown in table 3, the form of the polynomial being $\alpha_0 Z_H{}^2 + \alpha_1 Z_H + \alpha_2$. Table 3 shows that all three curves are very similar in shape (the α_0 and α_1 terms), which is the result expected upon inspection of figure 12. The most important difference between the curves occurs in the constant α_2 term which physically moves the fit to higher or

lower values of Z_{DR} for a constant Z_H . The corrected data set constant term gives the closest match to the background value; the uncorrected α_2 is negative, this being indicative of the effects of attenuation. An exact match is not expected because of natural variation in the DSD throughout the PPI.

8 Implications for attenuation correction at C-band

Attenuation by rainfall is much larger at C-band than at S-band, and because most European and Japanese operational networks use C-band the need for a method of correcting for attenuation at C-band is much more pressing. As a first step to exploring how the K_{DP} /A_{H-V} S-band algorithm would function at C-band figure 13 displays the relative contribution of different raindrop sizes to the various forward scattering amplitudes for a Marshall and Palmer (1948) DSD with a rainfall rate of 100mmhr^{-1} . If the curves were identically shaped then a single relationship would link K_{DP} with A_H as proposed by Bringi *et al.* (1990). At C-band the position of the peaks of the three curves are less consistent than at S-band; the K_{DP} curves are similar for the two wavelengths, but the attenuation is weighted more towards larger drops at C-band compared with S-band. However, for drops larger than 6mm the shapes of the C-band curves are more consistent. The sensitivity to μ, the index in the gamma function, is far lower at C-band, as demonstrated by figure 14, showing that the A_H versus A_{H-V} curves for μ=0 and μ=5 are almost identical at C-band.

Ideally C-band polarisation data should be used to assess the efficiency of the proposed correction scheme. Such data is not available to us, so our first step in assessing the efficiency of the correction algorithm at C-band was to use the S-band data to simulate attenuated C-band data. This was achieved by taking a ray of attenuated S-band data to ensure that appreciable attenuation is observed at C-band. The S-band data was first corrected for attenuation using the method outlined in section 6. S-band values of Z_H and Z_{DR} at each gate were then converted to C-band values assuming the precipitation was rain; this involves calculating N_0 D_0 at each gate using the standard technique of Seliga and Bringi (1976). If hail contaminates Z_H and Z_{DR} these N_0 and D_0 values will be spurious, but because both C- and S-band will both be contaminated, the C-band Z_H and Z_{DR} should be adequately simulated for our purpose.

However, in order to simulate the values of A_H , K_{DP} and δ (the differential phase shift on backscatter) at C-band, only the regions where there was appreciable attenua-

tion at S-band were used. The N_0 D_0 values derived from the observed A_{H-V} , K_{DP} at S-band were used to calculate these C-band parameters. This should ensure that the calculated attenuation is only due to the rain component of the precipitation.

The predicted C-band data for the S-band data in figure 10 is displayed in figure 15. The Z_{DR} behind the intense region of precipitation has reached -5dB which indicates that throughout the ray 5dB of differential attenuation has occurred (*cf.* 20dB of A_H). This compares with 1.5dB for the equivalent S-band ray shown in figure 10. Using the linear relationships proposed by Bringi *et al.* (1990) to act as a rough guide, A_{H-V} at C-band should be a factor of four greater than at S-band. This implies that the values of negative C-band Z_{DR} are of the correct order of magnitude.

The simulated C-band ϕ_{DP} data shows a change of greater than 100° over a range of 4km. The feature of note also is the transient spike of δ which occurs at a range of 30km which has a magnitude of $\sim$+15° . δ contributes to ϕ_{DP} throughout the large differential phase shift region, it is only when the beam emerges from the intense precipitation core that the characteristic spike is observable. In practice ϕ_{DP} ray profiles at C-band tend to be noisier than this (Bringi *et al.*, 1991) .

There are difficulties in adjusting the scheme to cope with the addition of δ , the largest problems occurring at the gates where the ray enters and subsequently emerges from the high D_0 rain shaft. (In the simulated data shown in figure 15, δ adds a constant offset to ϕ_{DP} , this being due to the value of D_0 being prescribed for the whole attenuating region by the scheme, which is perhaps unrealistic.) K_{DP} at these gates is therefore spurious and, as a consequence, the weightings calculated using the values of K_{DP} are incorrect throughout the attenuating rain shaft. The use of K_{DP} and A_{H-V} to calculate A_H are also compromised; the result being that A_H is hugely overestimated. The scheme therefore needs to be modified to cope with the significant contribution from δ .

As there is a significant amount of random noise associated with the measurement of ϕ_{DP} , it is necessary to smooth the ϕ_{DP} parameter so that K_{DP} can be extracted. Within the attenuation correction code a fourth order Butterworth filter (Parks and Burns, 1987) using a sampling rate of one tenth the original data is utilised for this purpose. This filter can smooth out the jump in ϕ_{DP} at the entry and emergent range gates and is also effective when a δ spike is present over a limited number of gates. This allows the weightings to be correctly assigned, but the actual values of K_{DP} ,

and hence the calculated values of A_H , are incorrect in this case where δ is adding a constant offset to ϕ_{DP} .

The attenuation correction algorithm therefore needs to be modified for use at C-band. The step involving the weightings can still be used, but an alternative to using K_{DP} and A_{H-V} to calculate N_0 and D_0, and hence A_H , needs to be found.

The algorithm can be modified to accommodate the determination of A_H when the K_{DP} signal is contaminated by δ by using a lookup table to derive the A_H from A_{H-V} . (Figure 6 suggests that there are not the problems in relating the two attenuation parameters to one another as there are in relating them to K_{DP} . The relationship between A_H and A_{H-V} should be relatively independent of N_0.)

Figure 14 shows that there is a dependency upon the value of μ in the DSD; the differences may not appear to be large but as they add cumulatively along a ray then an error of 0.2dBkm^{-1} could result in an overall error in the estimation of Z_H of 2dBZ over a 10km precipitation path length at C-band, and would clearly be worse for very extensive echoes. This error is quite small though when compared with the difference between the unattenuated C-band data and the corrected fields, shown in figure 16.

At this point a definition of terms is required. The *unattenuated* data is the C-band ray directly calculated from the corrected S-band Z_H and Z_{DR} ; this is used as "truth" against which to test the attenuation correction schemes. The *attenuated* data is the same ray but with the calculated A_H and A_{H-V} subtracted from Z_H and Z_{DR} respectively; it is this ray which is used as the input to the C-band correction scheme. The *attenuation corrected* data is the output from the correction scheme.

The scheme run without the modification to account for δ (dashed line in figure 16) shows an overestimation of 8dBZ in the Z_H field. This will lead to a serious overestimation of the rainfall rate in the regions behind the precipitation core which is causing the attenuation. When the lookup table modification is included the algorithm gives values of Z_H to within 1dBZ of the unattenuated data. The attenuation corrected Z_{DR} fields correspond well with the unattenuated data although there is a difference of (~1dB) within the precipitation core suggesting that the distribution of the correction is not altogether accurate within this region.

If it is correct to assume that at C-band A_H and A_{H-V} are linearly related then the C-band algorithm could be quite simple. The values of total attenuation could be derived from the differential attenuation (i.e., negative Z_{DR}) observed behind the

intense precipitation. This relies on the insensitivity of the A_H -A_{H-V} relationship to changes in μ (figure 14).

In addition we note that the most severe cases of attenuation result from heavy rain having exceptionally large sized drops. Figure 9 shows that the values of D_0 are 3 or 4mm, and lie along the curve for N_0=800m^{-3}mm^{-1}. Comparison of figures 4 and 5 shows that for this value of N_0 the value of differential attenuation is about 75% of the horizontal attenuation. This suggests that if only one polarisation is available for an operational radar then the vertical polarisation would be preferable, because the attenuation would only be about one third of the value for horizontal polarisation. The UK currently use vertical polarisation (Fair *et al.*, 1990) but so far as we can ascertain they are alone in this. Presumably horizontal polarisation has generally been chosen because there is slightly less ground clutter for this polarisation as demonstrated by its predominantly negative values of differential reflectivity Hall *et al.* (1984).

9 Conclusions

Previously, attenuation correction schemes have relied upon gate-by-gate iterative methods which quickly become unstable. These methods also rely upon backscatter parameters such as Z_H and Z_{DR} which can become contaminated with hail within the volume. Hail is indistinguishable from rain when single parameter radar is used but should produce much less attenuation because of its low concentration. Therefore when hail is present the correction schemes may be needlessly implemented resulting in overcorrection.

A new attenuation correction algorithm has been developed which makes use of the total amount of A_{H-V} at the back of the storm, determined by the magnitude of the negative Z_{DR} in the regions of light precipitation, and the measured ϕ_{DP} . The scheme has been implemented at S-band and, using raingauge and statistical validation, found to accurately correct for attenuation. In this work it was assumed that the rain causing the attenuation was at 20°C . Generally, because attenuation is temperature dependent, different look-up tables need to be generated for different temperatures. The advantages of the scheme are that it is numerically stable and relatively insensitive to hail. Simpler methods using K_{DP} alone do not provide a unique solution. Ryzhkov and Zrnić (1994) observed a differential attenuation which was twice as much as that predicted from K_{DP} by Bringi *et al.* (1990) and suggested that this was due to half melted ice cores. The

calculations and observation suggest that this higher attenuation for a given K_{DP} is due to the larger raindrops, and that Bringi *et al.* (1990) underestimated the attenuation by limiting the maximum value of D_0 to 2.5mm.

Implementation of the combined ϕ_{DP} Z_{DR} technique at C-band is more difficult because at this shorter wavelength there is more differential phase shift on backscatter by the large oblate raindrops. This backscatter phase shift is a transient superposed on the propagation phase and makes the propagation component more difficult to estimate. However it seems that at C-band the differential attenuation is more closely related to the total attenuation that at S-band. This suggests that a simpler algorithm may be implemented in which the total attenuation is simply related to the total differential attenuation which is found from the magnitude of the negative Z_{DR} in low intensity precipitation regions at greater range. It is suggested by these studies that this algorithm is not temperature dependent because the ratio of total to differential attenuation varies little with temperature. Further work is needed to confirm this suggestion.

The implementation of polarisation diversity involves the installation of a fast switch so that pulses can be transmitted alternately with horizontal and vertical polarisation. The implications for dwell time and scanning rates are discussed in Sachidananda and Zrnić (1985). In all these attenuation algorithms it is assumed that the radar beam is sampling at levels below the zero degree isotherm and is in the rain or hail rather than the ice above the melting layer. Since nearly all severely attenuating storms occur in the summer this should not be too severe a restriction, but clearly does place a limit to the absolute maximum range for the technique. Finally we note that if polarisation diversity is not available, then it is preferable to use vertical polarisation as the attenuation is much reduced when compared to that occurring in the horizontal.

10 Acknowledgements

This work was supported by NERC "HYREX" grant GST/02/718.
We thank the RCRU group at RAL for allowing access to the Chilbolton radar.
Jothiram Vivekenanden (NCAR) provided the scattering code.

References

Atlas, D., Harper, W. G., Ludlam, F. H., and Macklin, W. C. (1960). Radar scatter by large hail. *Quart. J. Roy. Meteor. Soc.*, **86**, 468–482.

Aydin, K., Seliga, T., and Balaji, V. (1986). Remote sensing of hail with a dual linear polarisation radar. *J. Climate Appl. Meteor.*, **25**, 1475–1484.

Aydin, K., Zhao, Y., and Seliga, T. A. (1989). Rain-induced attenuation effects on C-band dual-polarisation meteorological radars. *IEEE Trans. Geosci. Rem. Sens.*, **27**, 57–65.

Beard, K. V. and Chuang, C. (1987). A new model for the equilibrium shape of raindrops. *J. Atmos. Sci.*, **44**, 1509–1524.

Blackman, T. M. (1996). *Observations and interpretations of differential phase shift in precipitation using S- and K_A-band radars.* Ph.D. thesis, UMIST.

Bringi, V. N., Chandrasekar, V., Balakrishnan, N., and Zrnić, D. S. (1990). An examination of propagation effects in rainfall on radar measurements at microwave frequencies. *J. Atmos. Oceanic Technol.*, **7**, 829–840.

Bringi, V. N., Chandrasekar, V., Meischner, P., Hubbert, J., and Golestani, Y. (1991). Polarimetric radar signature of precipitation at S- and C- bands. *IEEE proc F*, **138**, 109–119.

Caylor, I. J. (1989). *Radar observations of maritime clouds using dual linear polarisation.* Ph.D. thesis, UMIST.

Cheng, L. and English, M. (1983). A relationship between hailstone concentration and size. *J. Atmos. Sci.*, **40**, 204–213.

Collier, C. G. (1990). *Radar in Meteorology. Ed. Atlas, D.*, chapter 29a Appendix A: Radar data processing and short-period forecasting in the United Kingdom, page 599. AMS, Boston, 1st edition.

Delrieu, G., Creutin, J. D., and Saint-Andre, I. (1991). Mean K-R relationships: Practical results for typical weather radar wavelengths. *J. Atmos. Oceanic Technol.*, **8**, 467–476.

Delrieu, G., Caoudal, S., and Creutin, J. D. (1997). Feasibility of using mountain return for the correction of ground-based X-band weather radar data. *J. Atmos. Oceanic Technol.*, **14**, 368–385.

Fair, C. A., James, P. K., and Larke, P. (1990). The United Kingdom weather network. In *Cost 73*, pages 147–154. Kluwer.

Goddard, J. W. F. and Cherry, S. (1984). Quantitative precipitation measurements of rain with ground-based distrometer measurements. In *22nd Conference on Radar Meteorology*, pages 352–357, Zurich, Switzerland. Amer. Met. Soc.

Goddard, J. W. F., Eastment, J. D., and Thurai, M. (1994). The Chilbolton advanced meteorological radar: a tool for multidisciplinary research. *Electronics & Communications Engineering J.*, **6**, 77–86.

Green, A. W. (1975). An approximation for the shape of large raindrops. *J. Appl. Meteor.*, **14**, 1578–1583.

Gunn, K. L. S. and East, T. W. R. (1954). The microwave properties of precipitation particles. *Quart. J. Roy. Meteor. Soc.*, **80**, 522–545.

Hall, M. P. M., Goddard, J. W. F., and Cherry, S. M. (1984). Identification of hydrometeors and other targets by dual-polarisation radar. *Radio Sci.*, **19**, 132–140.

Hildebrand, P. H. (1978). Iterative correction for attenuation of 5cm radar in rain. *J. Appl. Meteor.*, **17**, 508–514.

Hitschfeld, W. and Bordan, J. (1954). Errors inherent in the radar measurement of rainfall at attenuating wavelengths. *J. Meteorol.*, **11**, 58–67.

Illingworth, A. J. and Caylor, I. J. (1989). Polarisation radar estimates of raindrop size spectra and rainfall rates. *J. Atmos. Oceanic Technol.*, **6**, 939–949.

Jameson, A. R. (1983). Microphysical interpretation of multi-parameter radar measurements in rain: Part I interpretation of polarisation measurements and estimation of raindrop shapes. *J. Atmos. Sci.*, **40**, 1792–1802.

Jameson, A. R. (1992). The effect of temperature on attenuation-correction schemes in rain using polarization propagation differential phase shift. *J. Appl. Meteor.*, **31**, 1106–1118.

Kabeche, A. and Testud, J. (1995). Stereoradar meteorology: A new unified approach to process data from airborne or ground based meteorological radars. *J. Atmos. Oceanic Technol.*, **12**, 259–270.

Liebe, H. J., Manabe, T., and Hufford, G. A. (1989). Millimeter-wave attenuation and delay rate due to clouds/fog conditions. *IEEE AP*, **37**, 1617–1623.

Marshall, J. S. and Palmer, W. M. K. (1948). The distribution of raindrops with size. *J. Meteorol*, **6**, 243–248.

McCormick, G. C., Allan, L. E., and Hendry, A. (1979). The backscatter matrix of ice samples: its relation to the identification of hail by radar. *J. Appl. Meteor.*, **19**,

77–84.

O'Brien, S. G. and Geodecke, G. H. (1988). Scattering of millimetre waves by snow crystals and equivalent homogeneous symmetric particles. *Applied Optics*, **27**, 2439–2444.

Oguchi, T. (1973). Attenuation and phase rotation of radio waves due to rain: Calculations at 19.3 and 34.8GHz. *Radio Sci.*, **8**, 31–38.

Parks, T. W. and Burns, C. S. (1987). *Digital filter design*, chapter 7.3.3. John Wiley & Sons.

Pruppacher, H. R. and Pitter, R. L. (1971). A semi-empirical determination of the shape of cloud and raindrops. *J. Atmos. Sci.*, **28**, 86–94.

Ray, P. S. (1972). Broadband complex refractive indices of ice and water. *Appl. Opt.*, **11**, 1836–1844.

Ryzhkov, A. V. and Zrnić, D. (1994). Precipitation observed in Oklahoma Mesoscale Convective Systems with a polarimetric radar. *J. Appl. Meteor.*, **33**, 455–464.

Sachidananda, M. and Zrnić, D. (1985). Zdr measurement considerations for a fast scan capability radar. *Radio Sci.*, **20**, 907–922.

Sachidananda, M. and Zrnić, D. (1986). Differential propagation phase shift and rainfall estimation. *Radio Sci.*, **21**, 235–247.

Scarchilli, G., Gorgucchi, E., Chandrasekar, V., and Seliga, T. A. (1993). Rainfall estimation using polarimetric techniques at C-band frequencies. *J. Appl. Meteor.*, **32**, 1150–1160.

Seliga, T. A. and Bringi, V. N. (1976). Potential use of radar differential reflectivity measurements at orthogonal polarisations for measuring precipitation. *J. Appl. Meteor.*, **15**, 69–76.

Tan, J. (1995). Non-iterative algorithm to correct attenuation and differential attenuation effects on C-band polarisation-diversity radar measurements for improved rainrate estimation. In *Piers'95*, pages 24–28, Seattle, USA.

Ulbrich, C. W. (1983). Natural variations in the analytical form of the raindrop size distribution. *J. Climate Appl. Meteor.*, **22**, 1764–1775.

Waterman, P. C. (1965). Matrix formulation of electromagnetic scattering. *Proc. IEEE*, **53**, 805–812.

Wilson, D. R., Illingworth, A. J., and Blackman, T. M. (1997). Differential doppler velocity: A radar parameter for characterising hydrometeor size distributions. *J.*

Appl. Meteor., **36**, 649–663.

Captions

Table 1: S-band variation of A_H , N_0 and D_0 for a fixed value of A_{H-V} (0.25dBkm^{-1}) and variable K_{DP} at 20°C for $\mu = 0$. For consistency see figures 4 and 5.

Table 2: As table 1 but for $\mu = 2$.

Table 3: Coefficients of the second order polynomial fits shown in figure 12 d) for Z_{DR} as a function of Z_H .

Figure 1: Compensation effect at C-band using Beard and Chuang (1987) shapes and Marshall-Palmer dsd at T=0°C .

Figure 2: PPI of a)ϕ_{DP} , b)Z_H & c)Z_{DR} on 7/6/96 at 1936:09UTC; g5 and g7 are raingauge positions.

Figure 3: S-band comparison between hail and MP rain at 0°C . λ from 13 is varied between 0.1 and 2mm^{-1} for all hailstone compositions.

Figure 4: S-band K_{DP} as a function of A_H using Beard and Chuang (1987) shapes at 20°C , using different values of N_0 in the DSD (μ=0). The N_0 =8m^{-3}mm^{-1} line is shorter as all the data points for D_0 varying between 0 and 10mm are contained within the axis bounds.

Figure 5: K_{DP} as a function of A_{H-V} as for figure 4.

Figure 6: S-band variation of the forward scattering amplitude as a function of diameter at 20°C using Beard and Chuang (1987) shapes.

Figure 7: The variation of the forward scatter coefficient as a function of temperature and diameter at S-band using Beard and Chuang shapes and the dielectric constant of water.

Figure 8: Flow diagram of the attenuation correction scheme.

Figure 9: A_H as a function of K_{DP} for μ=0 (T=20°C). The data points are taken from several scans on the 7 June 1996 as part of the correction scheme.

Figure 10: Fields along a ray showing the measured and attenuation corrected Z_H and Z_{DR} . Azimuth 269.6° at 19:36GMT; gauge 7 is at a range of 32.2km.

Figure 11: Rainfall rates at gauges 5 and 7 during the time of the PPI shown in figure 2. The stars delimit the start and finish time of the PPI scan; the time resolution of the gauges is 10 seconds.

Figure 12: Z_H , Z_{DR} scatterplots showing a) "background" unattenuated azimuths b) uncorrected attenuated azimuths c) attenuated azimuths following attenuation correction d) comparison between the polynomial fits for the scatterplots. All for PPI

shown in figure 2.

Figure 13: a) Marshall and Palmer (1948) dsd for a rainfall rate of 100mmhr^{-1} ; b) Normalised imaginary part of the forward scatter matrix in the horizontal at S- and C-band (indicative of A_H), weighted by the dsd shown in a); c) as for b) except indicative of A_{H-V} ; d) as for b) except indicative of K_{DP} . All at 0°C and R=100mmhr^{-1} and values normalised by dividing by the maximum of the function.

Figure 14: S-band and C-band A_H as a function of A_{H-V} at 20°C for μ 0 & 5 in a normalised gamma dsd. N_0=8000m^{-3}mm^{-1}.

Figure 15: Ray along azimuth 268.9° showing the attenuated values of Z_H and Z_{DR} and the ϕ_{DP} data simulated at C-band.

Figure 16: Comparison between the original attenuation correction scheme proposed by this work (dashed), the modified scheme which uses a lookup table for A_H (solid) and the unattenuated data (dash-dot). The data is along the same azimuth shown in figure 15, at C-band.

Tables

K_{DP} (° km^{-1})	A_H (dBkm^{-1})	N_0 ($m^{-3}mm^{-1}$)	D_0(mm)
11	0.34	600	4.00
13	0.35	1050	3.73
15	0.37	1660	3.53
17	0.39	2440	3.37
19	0.41	3420	3.24

Table 1:

K_{DP} (° km^{-1})	A_H (dBkm^{-1})	N_0 ($m^{-3}mm^{-1}$)	D_0(mm)
11	0.34	165	4.61
13	0.35	270	4.34
15	0.37	410	4.14
17	0.38	580	3.98
19	0.40	790	3.85

Table 2:

Data set	α_0	α_1	α_2
Background	0.0011	-0.0112	0.3701
Uncorrected	0.0011	-0.0098	-0.1812
Corrected	0.0009	0.0036	0.2214

Table 3:

Figures

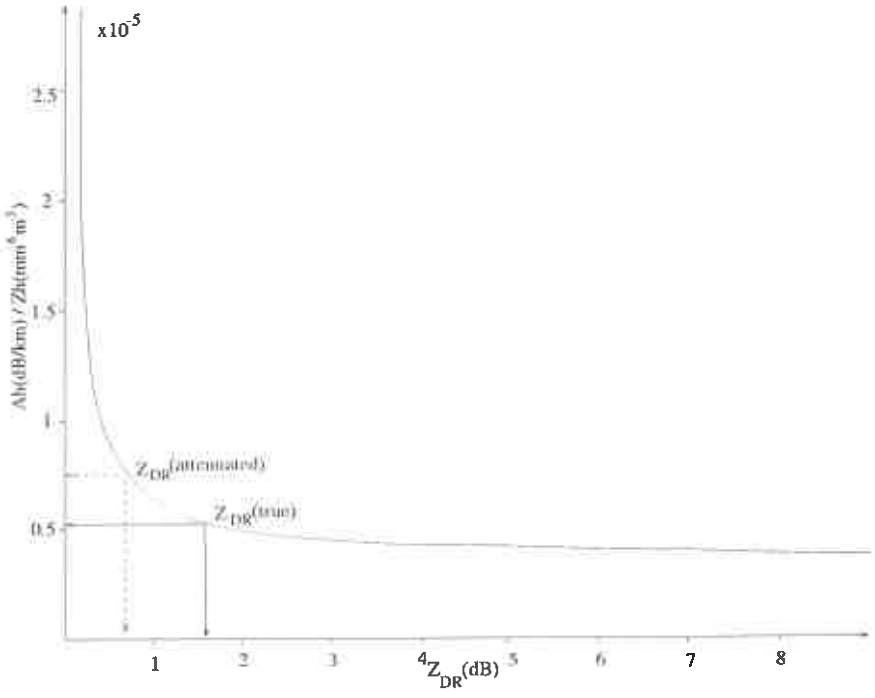

Figure 1:

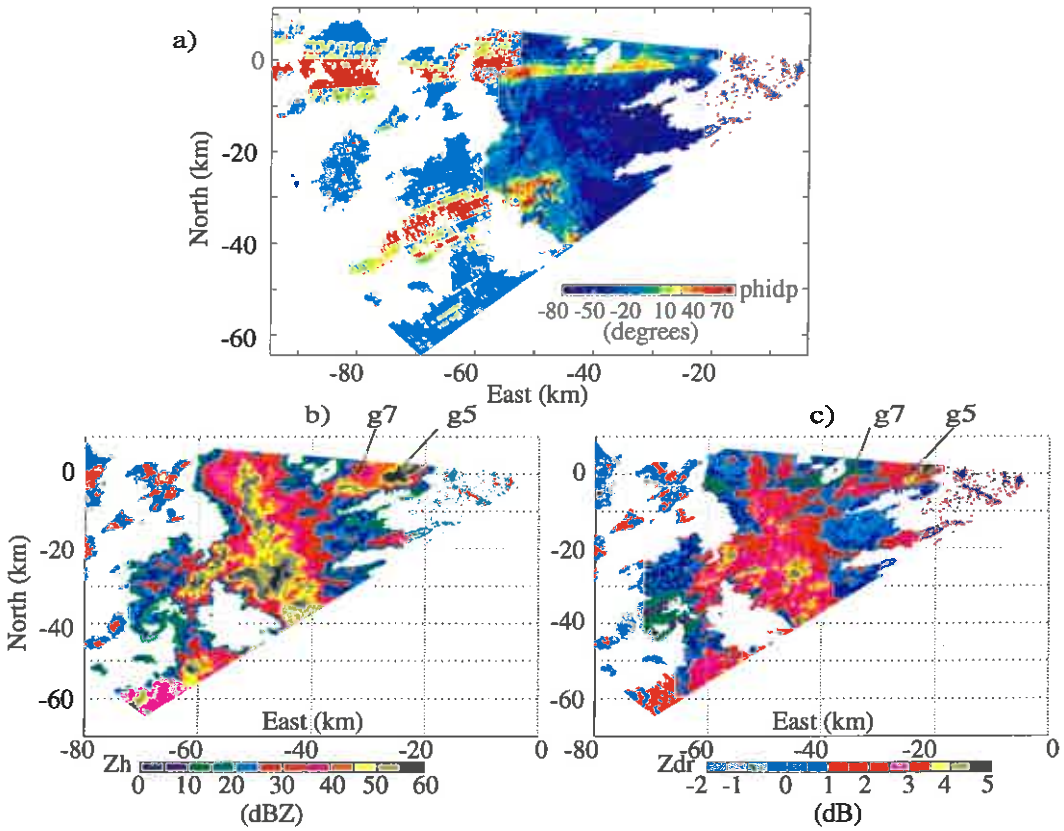
a)
North (km)
East (km)
phidp
-80 -50 -20 10 40 70
(degrees)
b)
g7
g5
Zh
0 10 20 30 40 50 60
(dBZ)
c)
Zdr
-2 -1 0 1 2 3 4 5
(dB)

Figure 2:

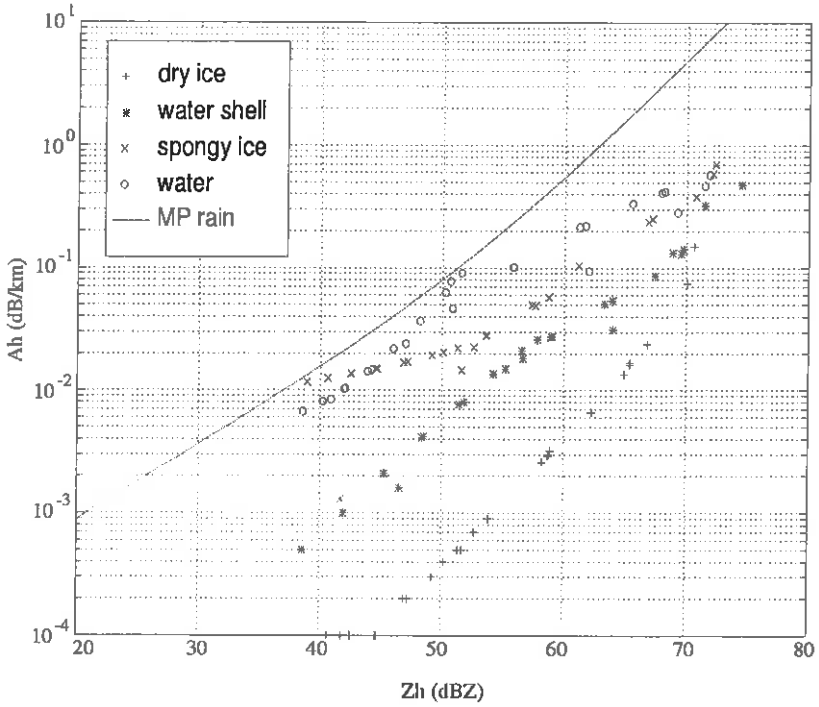

Figure 3:

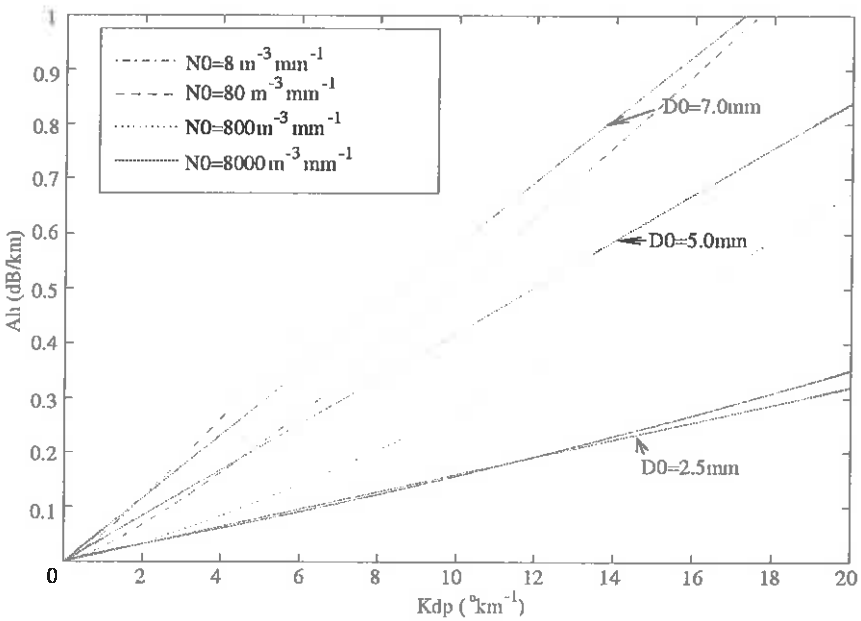

Figure 4:

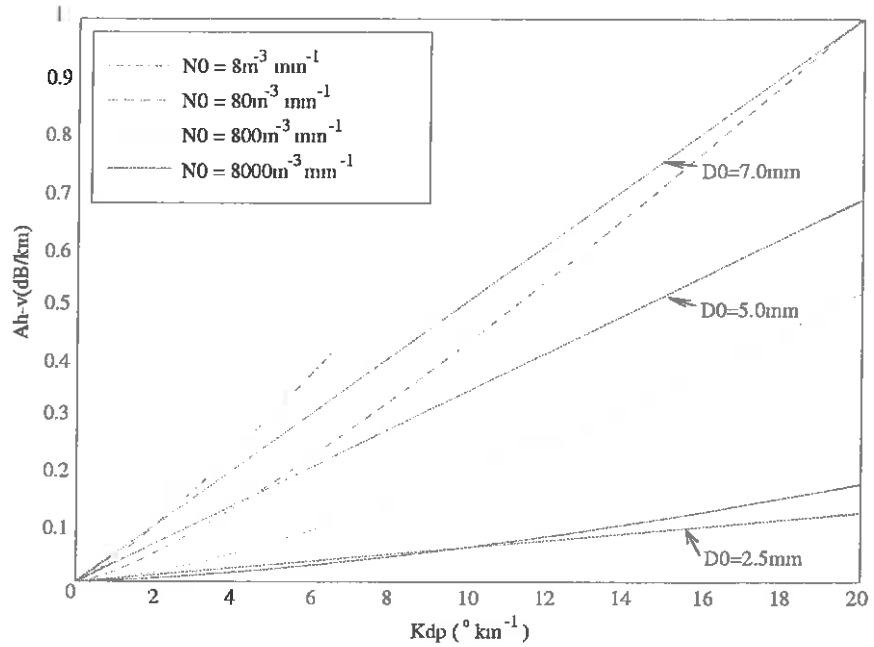

Figure 5:

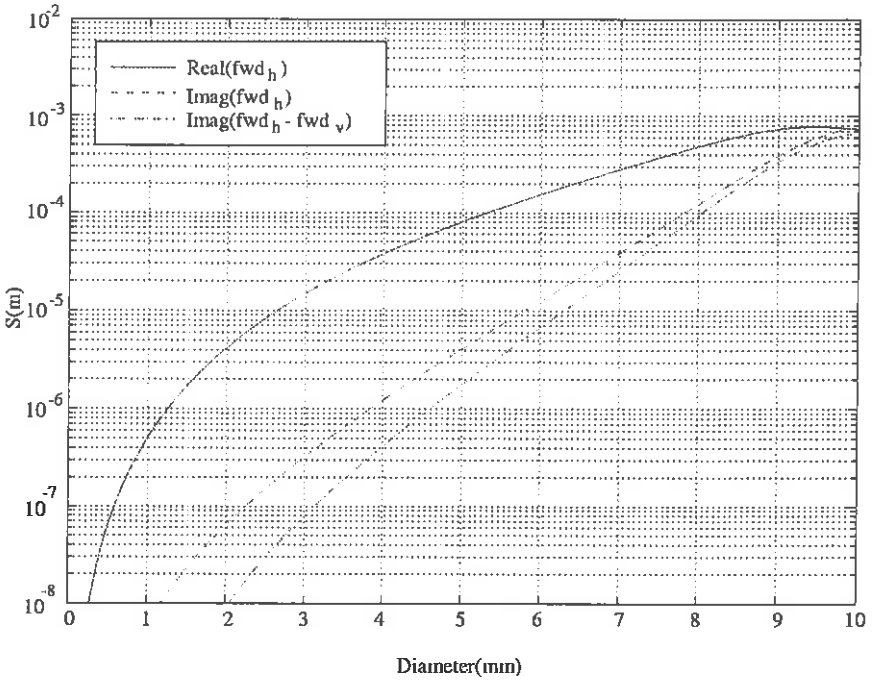

Figure 6:

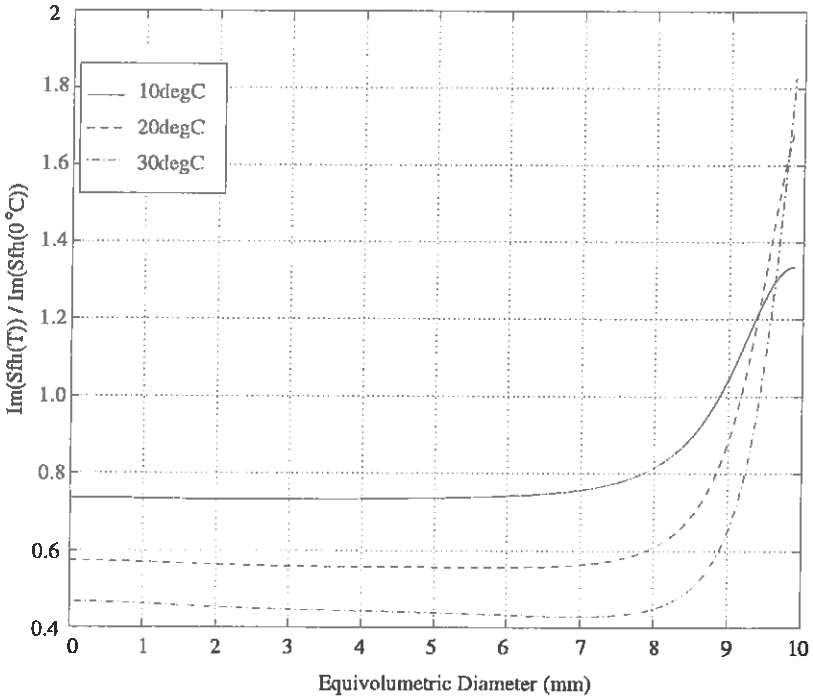

Figure 7:

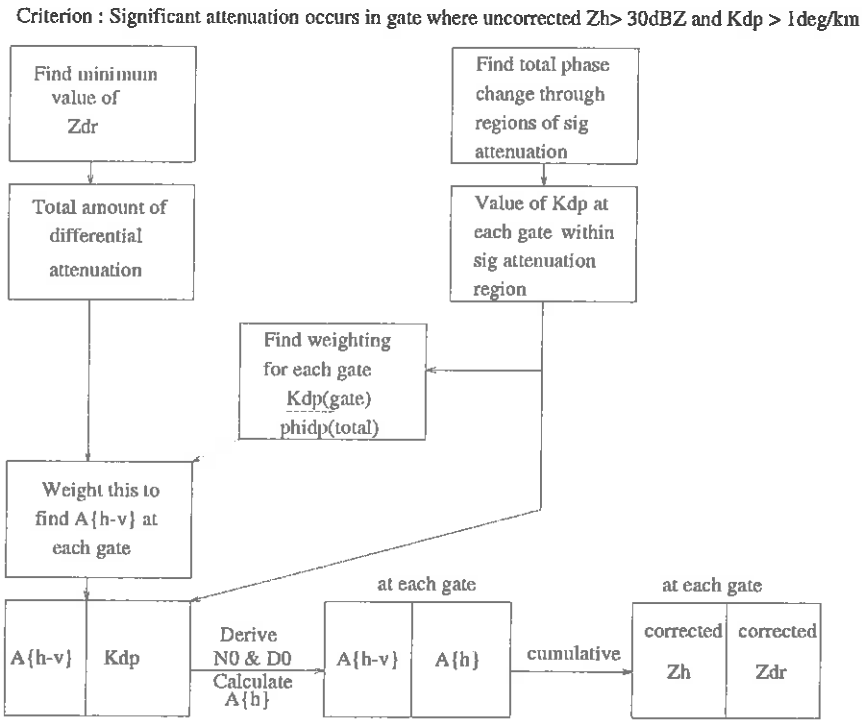

Figure 8:

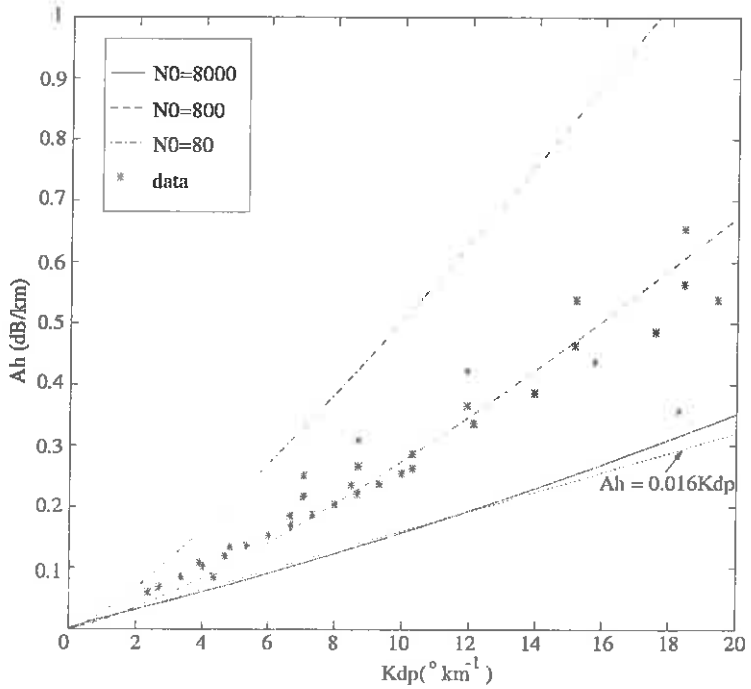

Figure 9:

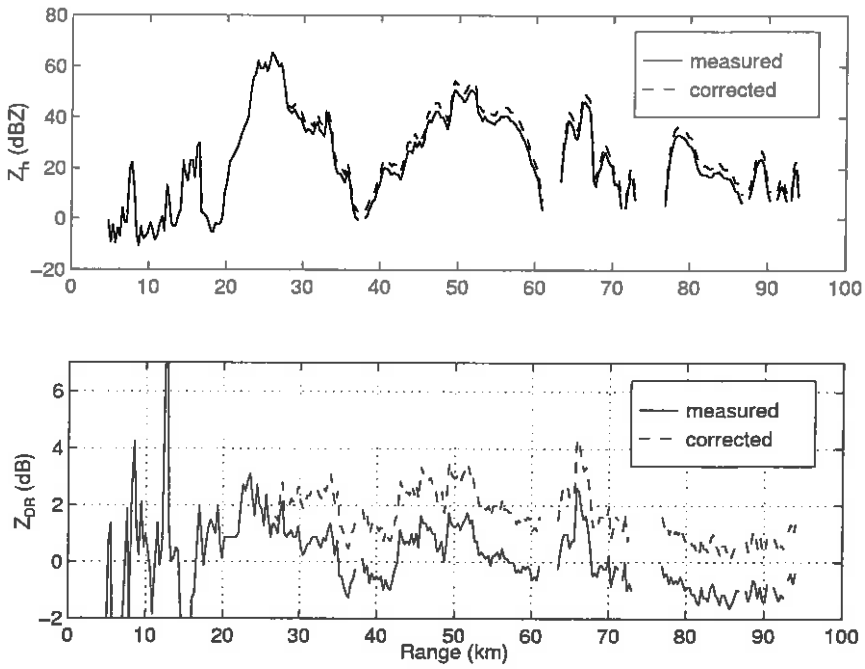

Figure 10:

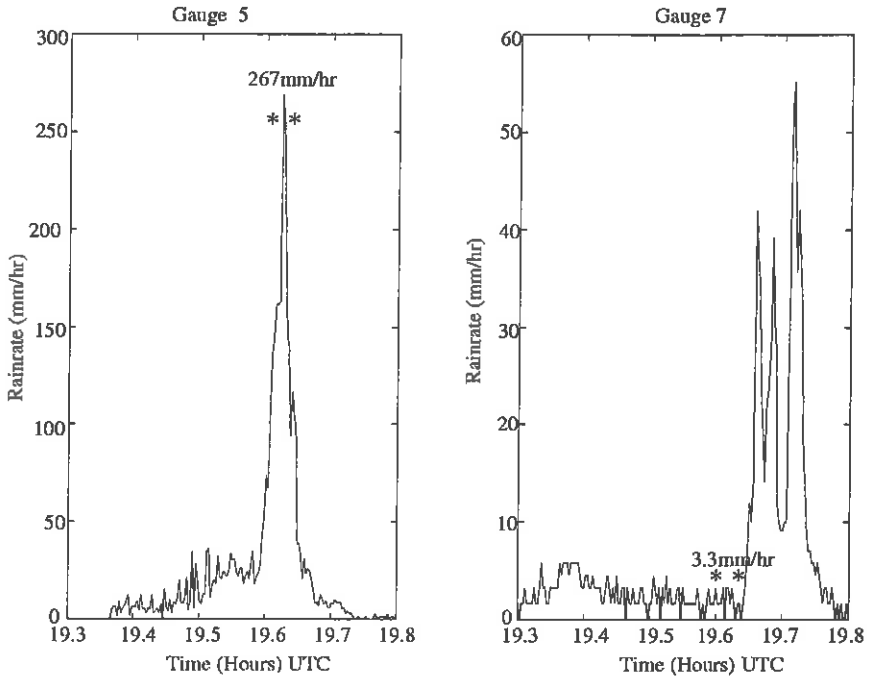

Figure 11:

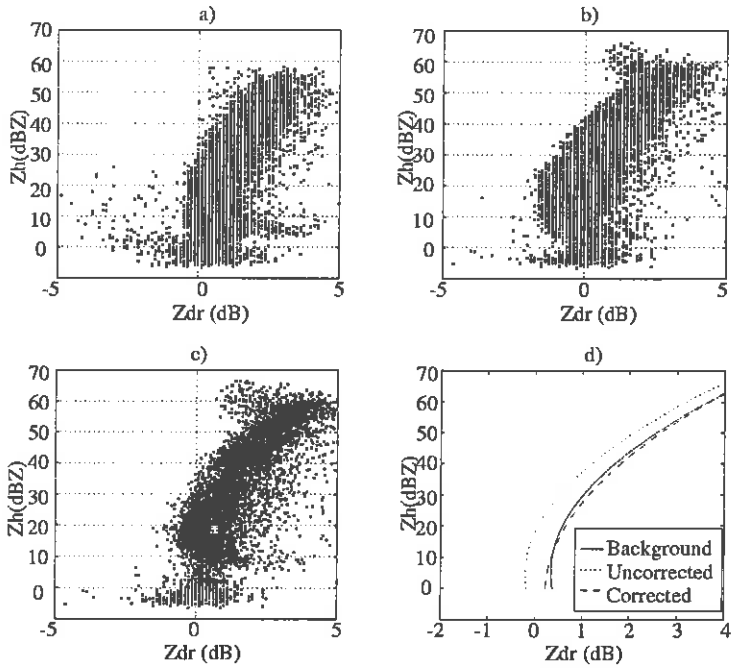

Figure 12:

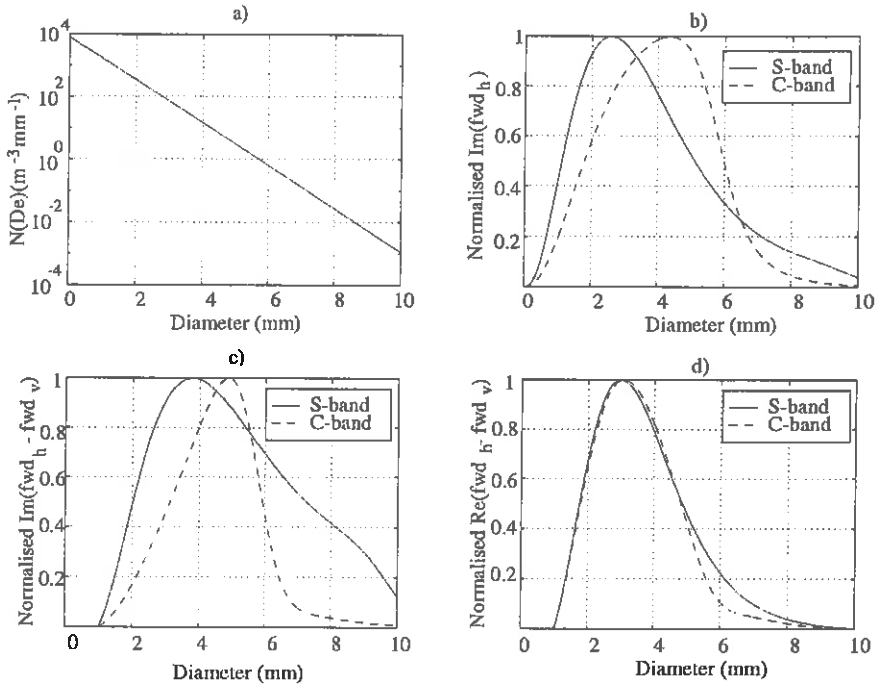
a)
b)
c)
d)
N(De)(m-3mm-1)
Normalised Im(fwd h)
Normalised Im(fwd h - fwd v)
Normalised Re(fwd h- fwd v)
Diameter (mm)
S-band
C-band

Figure 13:

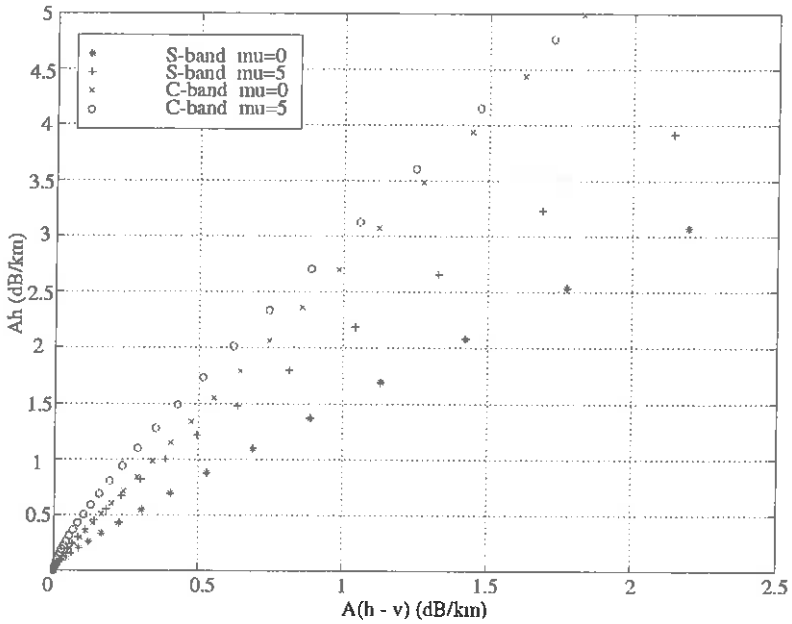
S-band mu=0
S-band mu=5
C-band mu=0
C-band mu=5
Ah (dB/km)
A(h - v) (dB/km)
0
0.5
1
1.5
2
2.5
3
3.5
4
4.5
5

Figure 14:

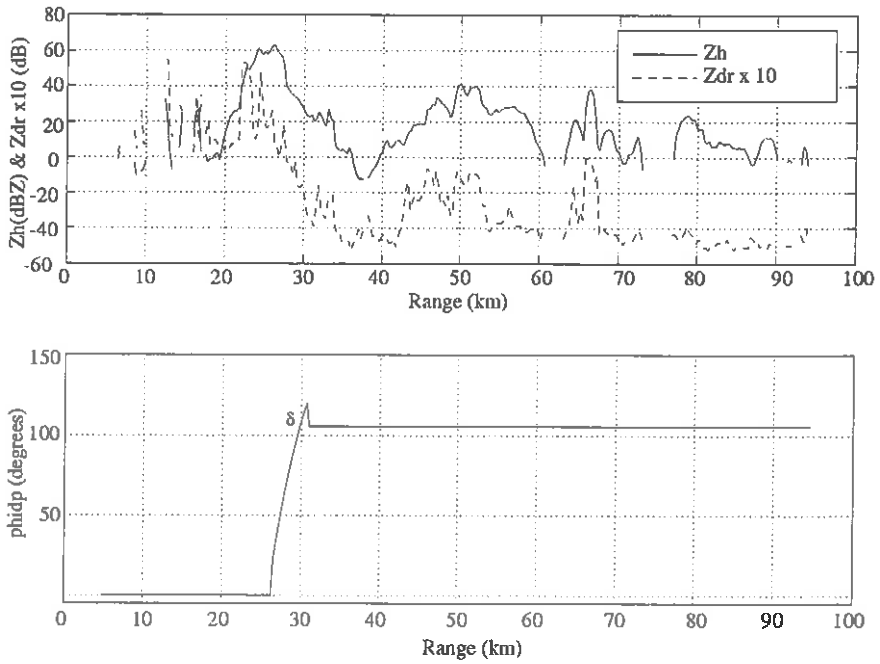

Figure 15:

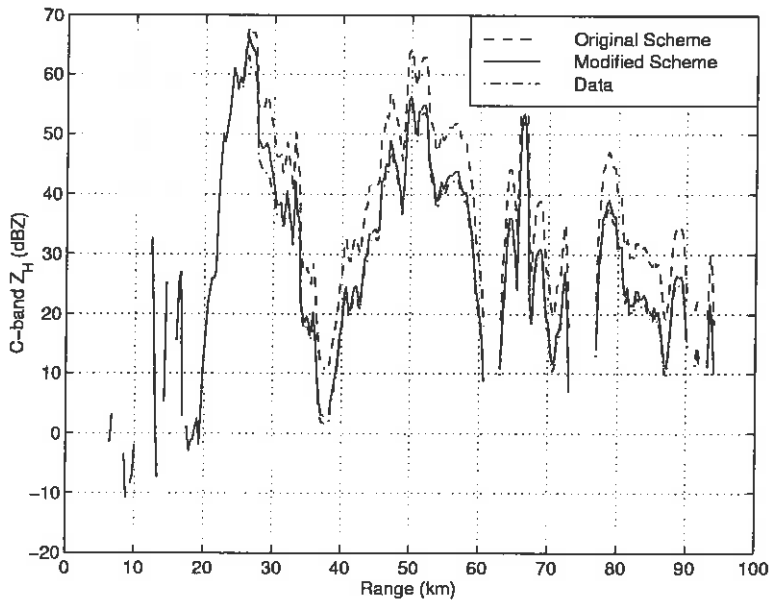

Figure 16:

CURRENT JCMM INTERNAL REPORTS

This series of JCMM Internal Reports, initiated in 1993, contains unpublished reports and also versions of articles submitted for publication. The complete set of Internal Reports is available from the National Meteorological Library on loan, if required.

1. **Research strategy and programme**
   K A Browning et al
   January 1993

2. **The GEWEX Cloud System Study (GCSS)**
   GEWEX Cloud System Science Team
   January 1993

3. **Evolution of a mesoscale upper tropospheric vorticity maximum and comma cloud from a cloud-free two dimensional potential vorticity anomaly**
   K A Browning
   January 1993

4. **The global energy and water cycle**
   K A Browning
   July 1993

5. **Structure of a midlatitude cyclone before occlusion**
   K A Browning and N Roberts
   July 1993

6. **Developments in systems and tools for weather forecasting**
   K A Browning and G Szejwach
   July 1993

7. **Diagnostic study of a narrow cold frontal rainband and severe winds associated with a stratospheric intrusion**
   K A Browning and R Reynolds
   August 1993

8. **Survey of perceived priority issues in the parametrizations of cloud-related processes in GCMs**
   K A Browning
   September 1993

9. **The effect of rain on longwave radiation**
   I Dharssi
   September 1993

10. **Cloud microphysical processes - a description of the parametrization used in the large eddy model**
    H Swann
    October 1993

11. **An appreciation of the meteorological research of Ernst Kleinschmidt**
    A J Thorpe
    May 1992

12. **Potential vorticity of flow along the Alps**
    A J Thorpe, H Volkert and Dietrich Heimann
    August 1992

13. **The representation of fronts**
    A J Thorpe
    January 1993

14. **A parametrization scheme for symmetric instability: test for an idealised flow**
C S Chan and A J Thorpe
February 1993

15. **The Fronts 92 Experiment: a Quicklook Atlas**
Edited by T D Hewson
November 1993

16. **Frontal wave stability during moist deformation frontogenesis**
Part 1: Linear wave dynamics
C H Bishop and A J Thorpe
May 1993

17. **Frontal wave stability during moist deformation frontogenesis**
Part 2. The suppression of non-linear wave development
C H Bishop and A J Thorpe
May 1993

18. **Gravity waves in sheared ducts**
S Monserrat and A J Thorpe
October 1993

19. **Potential vorticity and the electrostatics analogy: quasi-geostrophic theory**
C Bishop and A J Thorpe
November 1993

20. **Recent advances in the measurement of precipitation by radar**
A J Illingworth
April 1993

21. **Micro-physique et givrage: cloud microphysics and aircraft icing**
A J Illingworth
May 1993

22. **Differential phase measurements of precipitation**
M Blackman and A J Illingworth
May 1993

23. **Estimation of effective radius of cloud particles from the radar reflectivity**
N I Fox and A J Illingworth
May 1993

24. **A simple method of Dopplerising a pulsed magnetron radar**
A Hua, A J Illingworth and J Eastment
November 1993

25. **Radiation and polar lows**
George C Craig
February 1994

26. **Collected preprints submitted to the International Symposium on the Life Cycles of Extratropical Cyclones; Bergen, Norway, 27 June - 1 July 1994**
April 1994

27. **Convective frontogenesis**
Douglas J Parker and Alan J Thorpe
April 1994

28. **Improved measurement of the ice water content in cirrus using a total water evaporator**
Philip R A Brown and Peter N Francis
April 1994

29. **Mesoscale effects of a dry intrusion within a vigorous cyclone**
K A Browning and B W Golding
April 1994

30. **GEWEX Cloud System Study: Science Plan**
May 1994

31. **Parametrization of momentum transport by convectively generated gravity waves**
R Kershaw
May 1994

32. **Mesoscale Modelling Newsletter No 5**
May 1994

33. **Observations of the mesoscale sub-structure in the cold air of a developing frontal cyclone**
K A Browning, S A Clough, C S A Davitt, N M Roberts and T D Hewson
May 1994

34. **Longwave radiative forcing of a simulated tropical squall line**
Imtiaz Dharssi
July 1994

35. **On the nature of the convective circulation at a kata-cold front**
K A Browning
September 1994

36. **Collective preprints of papers submitted to the COST-75 International Seminar on Advanced Weather Radar Systems, Brussels, 20-23 September 1994**
November 1994

37. **Use of satellite imagery to diagnose events leading to frontal thunderstorms: Parts I and II of a case study**
K A Browning and N M Roberts
November 1994

38. **The role of spaceborne millimetre-wave radar in the global monitoring of ice cloud**
P R A Brown, A J Illingworth, A J Heymsfield, G M McFarquhar, K A Browning and M Gosset
December 1994

39. **Potential vorticity inversion**
Michal Ziemianski
October 1994

40. **Theory of mature tropical cyclones; a comparison between Kleinschmidt (1951) and Emanuel (1986)**
Suzanne L Gray
December 1994

41. **Dispersion and removal of pollutants during the passage of an atmospheric frontal system**
N R Gimson
December 1994

42. **The role of snow sublimation in frontogenesis**
D J Parker and A J Thorpe
December 1994

43. **Potential vorticity and the electrostatics analogy: Ertel-Rossby formulation**
A J Thorpe and C H Bishop
December 1994

44. **Mesoscale aspect of extratropical cyclones: an observational perspective**
K A Browning
January 1995

45. **A polar low outbreak: evolution and mesoscale structures**
T D Hewson, G C Craig and C Claud
February 1995

46. **Generation of near-surface gusts of deep convection**
K Nakamura and R Kershaw
April 1995

47. **Attribution concepts applied to the Omega Equation**
S A Clough, C S A Davitt and A J Thorpe
June 1995

48. **Parametrization of mixed-phase cloud and precipitation**
Susan P Ballard and M Gerard Hutchinson
June 1995

49. **Short-range forecasting of stratocumulus: initialization prediction**
Susan P Ballard, Simon D Jackson and B Macpherson
June 1995

50. **Contributions of the JCMM/Dept of Meteorology Radar Group to the 27th AMS Radar Meteorology Conference, Vail October 1995**
June 1995

51. **Cold pools in shear**
Douglas J Parker
September 1995

52. **High-resolution analysis of frontal fracture**
K A Browning, S P Ballard and C S A Davitt
September 1995

53. **The albedo of broken cloud fields: calculations using a modified two stream radiation code**
Imtiaz Dharssi and Roy Kershaw
October 1995

54. **Parametrization of momentum transport by convection. I: theory and cloud modelling results**
R Kershaw and D Gregory
November 1995

55. **Variation of frontal structure along a cold front**
K A Browning and N M Roberts
November 1995

56. **Secondary frontal waves**
Douglas Parker
December 1995

57. **Objective fronts**
T D Hewson
March 1996

58. **Mesoscale analysis of the activation of a cold front during cyclogenesis**
K A Browning, N M Roberts and A J Illingworth
June 1996

59. **Investigation of different representations of rain in a 1-d evaporation model**
H Swann
May 1996

60. **Parametrization of diabatic processes in the inversion of the omega-equation**
M Athanassiadou and A J Thorpe
June 1996

61. **The role of the environmental flow in the development of secondary frontal cyclones**
I A Renfrew, A J Thorpe and A Joly
June 1996

62. **Consequences of the geostrophic momentum approximation on barotropic instability**
S Malardel, A J Thorpe and A Joly
June 1996

63. **Contributions to the AMS/RMS Conference on Mesoscale Processes**
Reading, 9-13 September 1996

64. **Vorticity and potential vorticity in stratified flows interacting with an isolated obstacle**
Jorge A Gutiérrez and A J Thorpe
September 1996

65. **Triple point development: two case studies**
Douglas Parker
September 1996

66. **Radar observations of wind-shear splitting within evolving atmospheric Kelvin-Helmholtz billows**
D Chapman and K A Browning
April 1997

67. **Cold frontal structure derived from radar wind profilers**
K A Browning, D Jerrett, J Nash, T Oakley and N M Roberts
May 1997

68. **The dry intrusion and its effect on the frontal, cloud and precipitation structure of extratropical cyclones**
K A Browning - Text of invited special lecture at the Spring Conference
of the Meteorological Society of Japan, University of Tsukuba, 22 May 1997

69. **Met. Office Unified Model data, diagnostic graphics programs, and other observational data available from the JCMM through the aegis of the Universities Weather Research Network (UWERN).** (Plus supplement)
Peter Panagi and Ed Dicks
June 1997

70. **Contributions of the JCMM/Dept of Meteorology Radar Group to the 28th AMS Radar Meteorology Conference.** Austin, Texas
September 1997

71. **Sensitivity of short-range weather forecasts to local potential vorticity modifications**
Meral Demirtas and Alan Thorpe
July 1997

72. **Objective identification of frontal wave cyclones**
T D Hewson
August 1997

73. **Attribution and its application to mesoscale structure associated with tropopause folds**
A J Thorpe
September 1997

74. **The role of the environmental flow in the development of secondary frontal cyclones**
Ian A Renfrew, Alan J Thorpe and Craig H Bishop
September 1997

75. **Potential vorticity: a short history of its definitions and uses**
Alan J Thorpe and Hans Volkert
September 1997

76. **Superposing semi-geostrophic potential vorticity anomalies**
H R Birkett and A J Thorpe
September 1997

77. **Short period forecasting of catchment-scale precipitation.**
Part 1: the role of Numerical Weather Prediction
M A Pedder, M Haile and A J Thorpe
September 1997

78. **Verification of the tracking technique used in an experimental cloud motion wind inferring system**
Z Wang, K A Browning and G A Kelly
October 1997

79. **A preliminary study of Fourier series analysis for cloud tracking with GOES high temporal resolution images**
Z Wang
October 1997

80. **Analysis of an ex-tropical cyclone after reintensifying as a warm-core extratropical cyclone**
K A Browning, G Vaughan and P Panagi
November 1997

81. **A JCMM overview of FASTEX IOPs**
S A Clough, H W Lean, N M Roberts, H Birkett, J-P Chaboureau, R Dixon, M Griffiths, T D Hewson and A Montani
January 1998

82. **Programs for PV inversion and modification**
Meral Demirtas
December 1997

83. **Release of potential shearing instability in warm frontal zones**
D Chapman and K A Browning
February 1998

84. **The European Cloud-Resolving Modelling Programme (EUCREM)**
Summary Report from the coordinator
P W White
April 1998

85. **A frontal wave database**
T D Hewson
April 1998

86. **Layering observed in dropsoundings from IOP 1 of Fronts 92**
S A Clough
May 1998

87. **Use of wind-shear displays for Doppler radar data**
D Chapman and K A Browning
May 1998

88. **Radar estimates of rainfall rates at the ground in bright band and non-bright band events**
T J Smyth and A J Illingworth
June 1998

89. **Correction for attenuation of radar reflectivity using polarisation data**
T J Smyth and A J Illingworth
June 1998

Met Office Joint Centre for Mesoscale Meteorology Department of Meteorology
University of Reading PO Box 243 Reading RG6 6BB United Kingdom
Tel: +44 (0)118 931 8425 Fax: +44 (0)118 931 8791
www.metoffice.com